Investigation of the Structure and Photoluminescence Properties of Ln $^{3+}$(Eu^{3+}, Dy^{3+}, Sm^{3+}) Ion-Doped $NaY(MoO_4)_2$

Qi Wu, Huaiyong Li, Wanwan Xia, Xihong Fu, Zuoling Fu, Shihong Zhou, Siyuan Zhang and Jung Hyun Jeong

J. Electrochem. Soc. 2011, Volume 158, Issue 12, Pages J387-J393.
doi: 10.1149/2.012112jes

Journal of The Electrochemical Society, **158** (12) J387-J393 (2011)
0013-4651/2011/158(12)/J387/7/$28.00 © The Electrochemical Society

Investigation of the Structure and Photoluminescence Properties of Ln^{3+}(Eu^{3+}, Dy^{3+}, Sm^{3+}) Ion-Doped $NaY(MoO_4)_2$

Qi Wu,[a,b] Huaiyong Li,[d] Wanwan Xia,[a,b] Xihong Fu,[e] Zuoling Fu,[a,b,z] Shihong Zhou,[c] Siyuan Zhang,[c] and Jung Hyun Jeong[d,z]

[a]*State Key Laboratory of Superhard Materials, College of Physics, Jilin University, Changchun 130012, China*
[b]*Key Lab of Coherent Light, Atomic and Molecular Spectroscopy, Ministry of Education, Changchun 130021, China*
[c]*State Key Laboratory of Rare Earth Resources Utilization, Changchun Institute of Applied Chemistry, Chinese Academy of Sciences, Changchun 130022, China*
[d]*Department of Physics, Pukyong National University, Busan 608-737, South Korea*
[e]*Changchun Institute of Optics, Fine Mechanics and Physics, Chinese Academy of Sciences, Changchun 130033, China*

Novel phosphors of $NaY(MoO_4)_2$ activated with the trivalent rare-earth Ln^{3+} (Eu^{3+}, Dy^{3+}, Sm^{3+}) ions were synthesized by facile hydrothermal method with further calcinations. The ultraviolet-visible and photoluminescence spectra of there compounds were characterized to study the optical properties. The electronic structure and orbital population of $NaY(MoO_4)_2$ were determined by means of density functional theory calculation. The $NaY(MoO_4)_2$:Ln^{3+} (Eu^{3+}, Dy^{3+}, Sm^{3+}) phosphors show strong light emissions with different colors coming from different Ln^{3+} ions under blue excitation, which can be used as a potential candidate for white-light-emitting diode and other display devices.
 [DOI: 10.1149/2.012112jes]

Manuscript submitted May 25, 2011; revised manuscript received August 31, 2011. Published November 1, 2011.

Rare earth (RE) ion doped phosphors have attracted great interest during the past several decades due to their unique physical and chemical properties.[1–3] Recently, the development of flat panel displays, such as field emission displays (FEDs), plasma display panels (PDPs) and thin film electro-luminescent devices (TFEL), or white light-emitting diodes (w-LEDs), have emerged as the principal motivation for research into rare-earth luminescence, and the present article therefore concentrates on the variety of different ways in which rare-earth luminescence has been exploited in this field.[4–7] The rare earth-molybdenum (VI) oxides system constitutes a very rich family within which a great variety of compounds can be synthesized which differ in stoichiometry and structure. Recently, many works focused on luminescence properties research of molybdates doped with rare earth ions also have been carried out[8–11] because molybdates have been widely used as host candidates for white LEDs. $MLn(MoO_4)_2$ (M = alkali metal, Ln = rare earth) molybdate crystals are attractive host materials, not only because of their large lanthanide admittance, but especially owing to their good optical properties.[12–16] The $MLn(MoO_4)_2$ single crystals, which is with a scheelite structure, can be used as self-doubling solid-state laser host materials.[12,17,18] In the fields of phosphor materials, $MLn(MoO_4)_2$ materials doping Eu or Tb also present excellent luminescent properties.[18,19] In Wang et al.'s[19] reports, it is interesting that no concentration quenching of Eu can be observed in the samples of $NaLn_{1-}Eu_x(MoO_4)_2$ and $LiEu(MoO_4)_2$ systems, both of which exhibit the strongest red emission under 395 nm light excitation and appropriate CIE chromaticity coordinates (0.66, 0.34) close to the NTSC standard values. To our knowledge, luminescence in Dy^{3+}, Sm^{3+}-doped $NaY(MoO_4)_2$ powders has not been reported. In this paper, Dy^{3+}, Sm^{3+} ions activated $NaY(MoO_4)_2$ were prepared by hydrothermal method besides Eu^{3+} ions, and the phases, morphologies, and photoluminescent properties were then studied. In addition, it is known that the physical properties of materials are closely related to their chemical composition, crystal structure and electronic structure, and density functional theory (DFT) calculations can offer us detailed information about atom and orbital arrangement, which can help us to understand the structure-property relationship better. Therefore DFT calculations were also carried out in this work to determine the crystal structure and electronic structure of the host $NaY(MoO_4)_2$.

Experimental

Synthesis of the samples.— Materials.— Lanthanide nitrate solutions were obtained by dissolving lanthanide oxide (99.99%) in dilute nitric acid solution under heating with agitation. All the other chemicals were of analytical grade and used as received without further treatment. For the hydrothermal treatment, we used 60 mL Teflon cups.

Synthesis.— In a typical procedure of preparing $NaY(MoO_4)_2$:Eu^{3+}, 20 ml 0.1 mol/L $Y(NO_3)_3$ and 1 mL of 0.8 mol/L $Eu(NO_3)_3$ were first added into test tube. Subsequently, 15 mL of aqueous solution containing 0.57 mmol of $(NH_4)_6Mo_7O_{24} \cdot 4H_2O$ was added into the above solution with strong magnetic stirring at room temperature for 10 minutes to form a homogeneous solution. Next, the same solutions were adjusted to pH = 4.5, 5, 5.5, 6, 7, 7.5 by adding

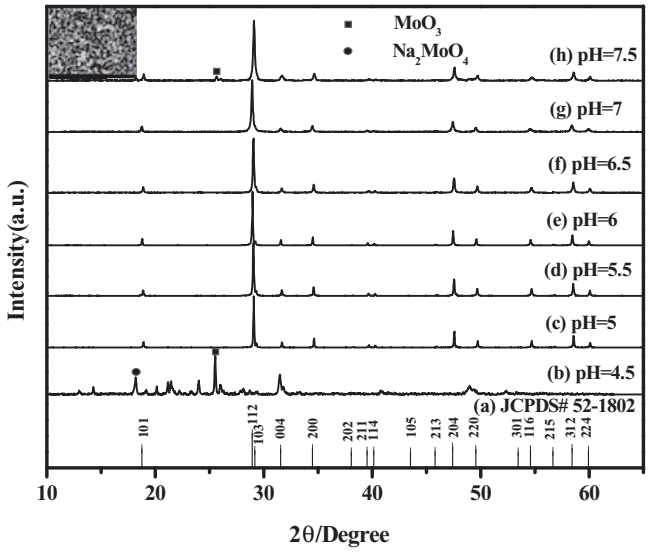

Figure 1. XRD powder patterns of $NaY(MoO_4)_2$:Eu^{3+} samples prepared by hydrothermal method at 180°C for 12 h at (b) pH = 4.5; (c) pH = 5; (d) pH = 5.5; (e) pH = 6; (f) pH = 6.5; (g) pH = 7; (h) pH = 7.5 with further calcination at 800 °C for 4 h.

[z] E-mail: zlfu@jlu.edu.cn; jhjeong@pknu.ac.kr

dropwise amount of NaOH (5M) into the above solution under vigorous stirring before hydrothermal treatment. The amount of NaOH was controlled by the showing of pH value on pH-meter(the Micro-Digit PH/mv Meter with high accuracy of ±0.01pH), still assisting with the diluted HNO_3 solution by adding dropwise when it was necessary. Then, NaOH immediately reacted with the molybdenum source and rare earth nitrate solutions, and a slurry-like white precipitate was formed. The mixture was stirred again for 1 h. Finally, the mixture was transferred in a Teflon bottle held in a stainless steel autoclave sealed and maintained at 180°C for 12 h. As the autoclave was cooled to room temperature naturally, the precipitate was filtered and washed with alcohol and deionized water several times. The precipitates were dried at 60°C for 12 h on air. The as-prepared products were retrieved through a heat treatment at 800°C in air for 4 h and then slowly cooled to room temperature. Finally, we can obtain $NaY(MoO_4)_2$:Eu^{3+} powders. For $NaY(MoO_4)_2$:Dy^{3+} and $NaY(MoO_4)_2$:Sm^{3+}, the detailed hydrothermal procedure is similar to Eu^{3+}-doped $NaY(MoO_4)_2$. In addition, it should be mentioned that the activators content (Eu^{3+}, Dy^{3+} and Sm^{3+}) was maintained at 4 mol % for the prepared samples.

Characterization.— The structure of the final products was examined by Powder X-ray diffraction (XRD) using Cu Kα radiation (λ = 0.15405 nm) on a Rigaku-Dmax 2500 diffractometer. A field emission-scanning electron microscope (FE-SEM, JSM-6700F, JEOL) was used to characterize the size and morphology of the synthesized $NaY(MoO_4)_2$ phosphors. For the optical investigation, the diffused reflectance spectra of the samples over a range for 190-700 nm was recorded by using a Uarian Cary 100 scan UV-Visible spectrophotometer equipped with a Labsphere diffuse reflectance accessory. The ultraviolet-visible photoluminescence (PL) excitation and emission spectra were recorded with a Hitachi F-7000 spectrophotometer equipped with Xe-lamp as an excitation source. All the measurements were performed at room temperature.

Calculations.— DFT calculations were performed on $NaY(MoO_4)_2$ by using CASTEP code.[20] For the properties calculation, the Vanderbilt ultrasoft pseudopotential,[21] which describes the interaction of valence electrons with ions, was used with the same cutoff energy of 340 eV. The 3 × 3 × 4 k-points were generated using the Monkhorst-Pack scheme.[22] The exchange and correlation functions were treated by the local density approximation (LDA) in the formulation of CA-PZ.[23,24] Valence electrons were described by using Vanderbilt-type nonlocal ultrasoft pseudopotentials while tightly bound core electrons were ignored.[25]

Results and Discussion

Crystal structure and morphologies.— Figure 1 shows the results of the XRD analysis of the hydrothermal reaction products obtained at 180°C for 12 h under different pH values with further calcination at 800°C for 4 h. Suitable pH value for the synthesis of single phase crystalline $NaY(MoO_4)_2$:Eu^{3+} powders was investigated by varying the base (NaOH) concentration used in the reaction system. When the value of pH < 5, some of Na_2MoO_4 and MoO_3 appeared as impurity(Figure 1b pH = 4.5), whereas beginning with pH = 5, no impurity peaks were detected in this experimental range (Figure 1c). All of the diffraction peaks can be indexed to the scheelite-type tetragonal structure (JCPDS no.52-1802) with $I4_1/a$ lattice symmetry. The lattice constants are calculated to be $a = b = 5.189$ Å and $c = 11.313$ Å. In addition, when the pH value varied from 5.5 to 7, we also can obtain the pure phase (Figure 1d-1g). When the value of pH = 7.5, trace MoO_3 appeared as impurity (Figure 1h). The above-stated results indicated that the pH value was very important for preparing the pure phase $NaY(MoO_4)_2$. We have also performed the FE-SEM measurement on the $NaY(MoO_4)_2$ powders, as shown in the inset of Figure 1. It was about 200 nm with regular distribution when the value of pH = 7(Sample (g)).

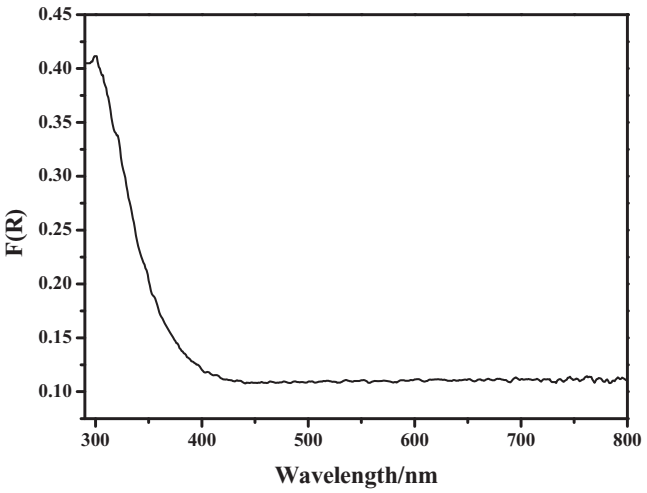

Figure 2. Diffused reflectance spectrum of $NaY(MoO_4)_2$ powders.

Energy gap, Band structure, and Density of State (DOS).— The diffused reflectance spectrum of $NaY(MoO_4)_2$ was measured and shown in Figure 2. The optical absorption can be used for estimating the band gap by using the Kubelka-Munk equation.[26] Kubelka-Munk's equation was described as follows: $F(R) = (1 - R)^2/2 = K/S$, where R, K and S were the reflectivity, the absorption, and the scattering coefficients, respectively. For $NaY(MoO_4)_2$, the absorption edge was around 378 nm (3.28 eV), which was similar to the other result of $Na_5Gd(MoO_4)_4$.[27]

To understand the chemical bonding properties and electronic origin of optical transition, the band structure and density of states were performed by the DFT method. The calculated band structures along the high symmetry points of the first Brillouin zone for $NaY(MoO_4)_2$ were shown in Figure 3a. We can see that the lowest energy of conduction bands (CBs) was localized at the G point, while the highest energy of valence bands (VBs) was also localized at the G point. Hence, $NaY(MoO_4)_2$ was a direct bandgap insulator. What's more, the gap between the lowest energy of the conduction band and the highest energy of the valence band was about 3.42 eV, which was comparable to the experimental value (3.28 eV). Figure 3b and 3c presented the density of states for the tetragonal $NaY(MoO_4)_2$ since the partial density of states (PDOS) was a useful tool to analyze the chemical bonding in solids. The upper valence band between −3.0 eV and the Fermi level (0.0 eV) was dominated by the O-2p, mixing with very small amount of Na-3s2p, Y-4d and Mo-4d5s states. The conduction band just above the Fermi level was dominated by Mo-4d states, with a slight contributions of the Y-4d and O-2p. Therefore, their optical absorptions at low energy region can be mainly ascribed to the charge transitions from O-2p to Mo-4d states.

Photoluminescent properties of $NaY(MoO_4)_2$:Eu^{3+}.— It is well known that the Eu^{3+} ion is a widely used luminescence activator with orange or red light emission, as well as a promising structural probe. The Eu^{3+} ion energy levels arise from the $4f^n$ configuration, and the transitions from excited $^5D_0$ level to ^7F_J (J = 0–6) levels result in its emission.

At the same level of Eu^{3+}, the phosphors $NaY(MoO_4)_2$ were prepared at various pH values and the evolution of the emission and excitation spectra as the increasing of pH values were presented in Figure 4. All spectra are similar in the shapes and locations excluding relative intensities. With the change of pH value from 5.5 to 7, the excitation and emission intensities increase gradually and reach maximum at pH = 7, which is consistent with the results of XRD and FE-SEM. The morphology and photoluminescence are optimal when pH = 7. The excitation spectra(Figure 4, left) are monitored at

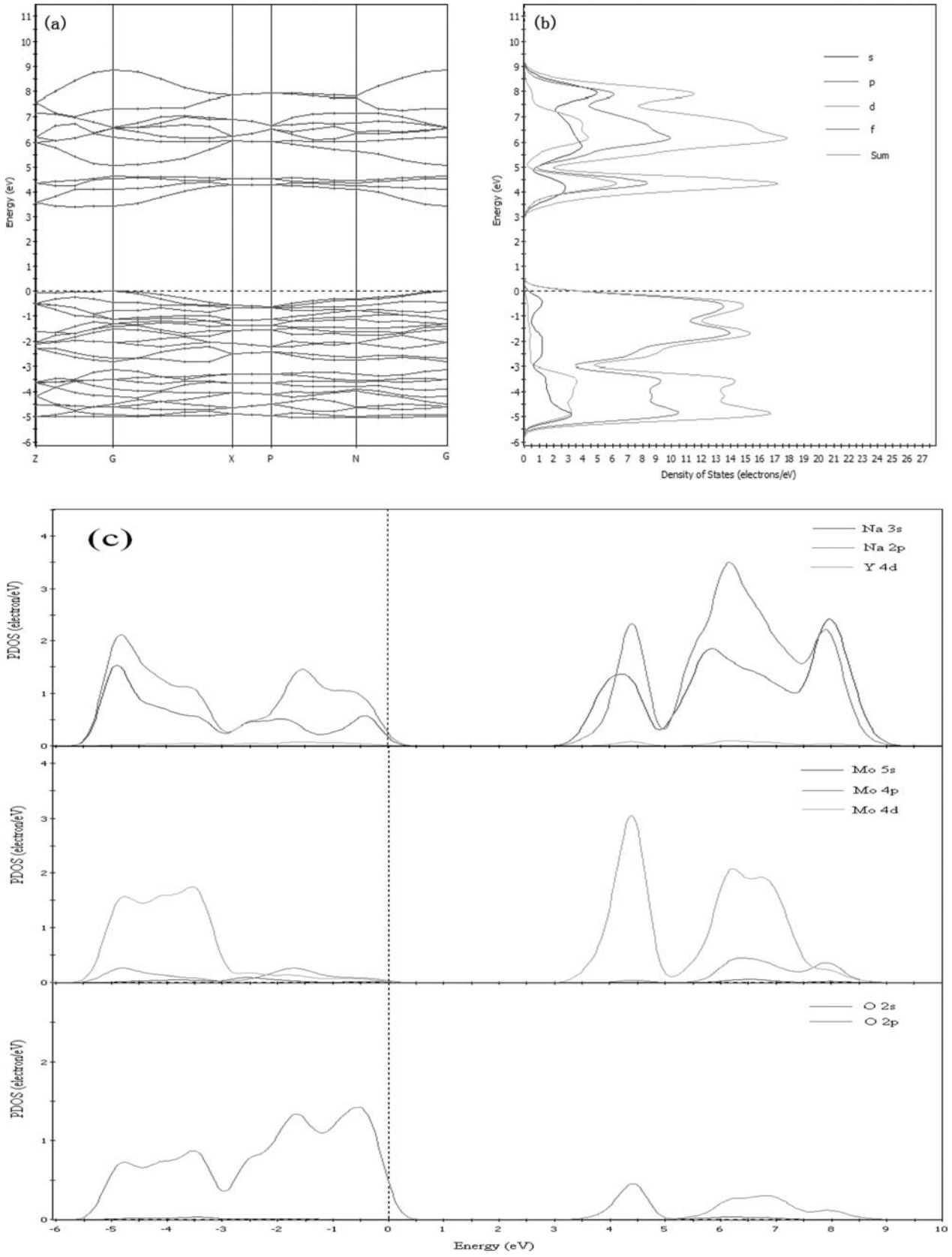

Figure 3. The calculated energy band structure(a); density of states (b) and partial DOS (c) of $NaY(MoO_4)_2$ near the Fermi energy level. The Fermi energy is the zero of the energy scale.

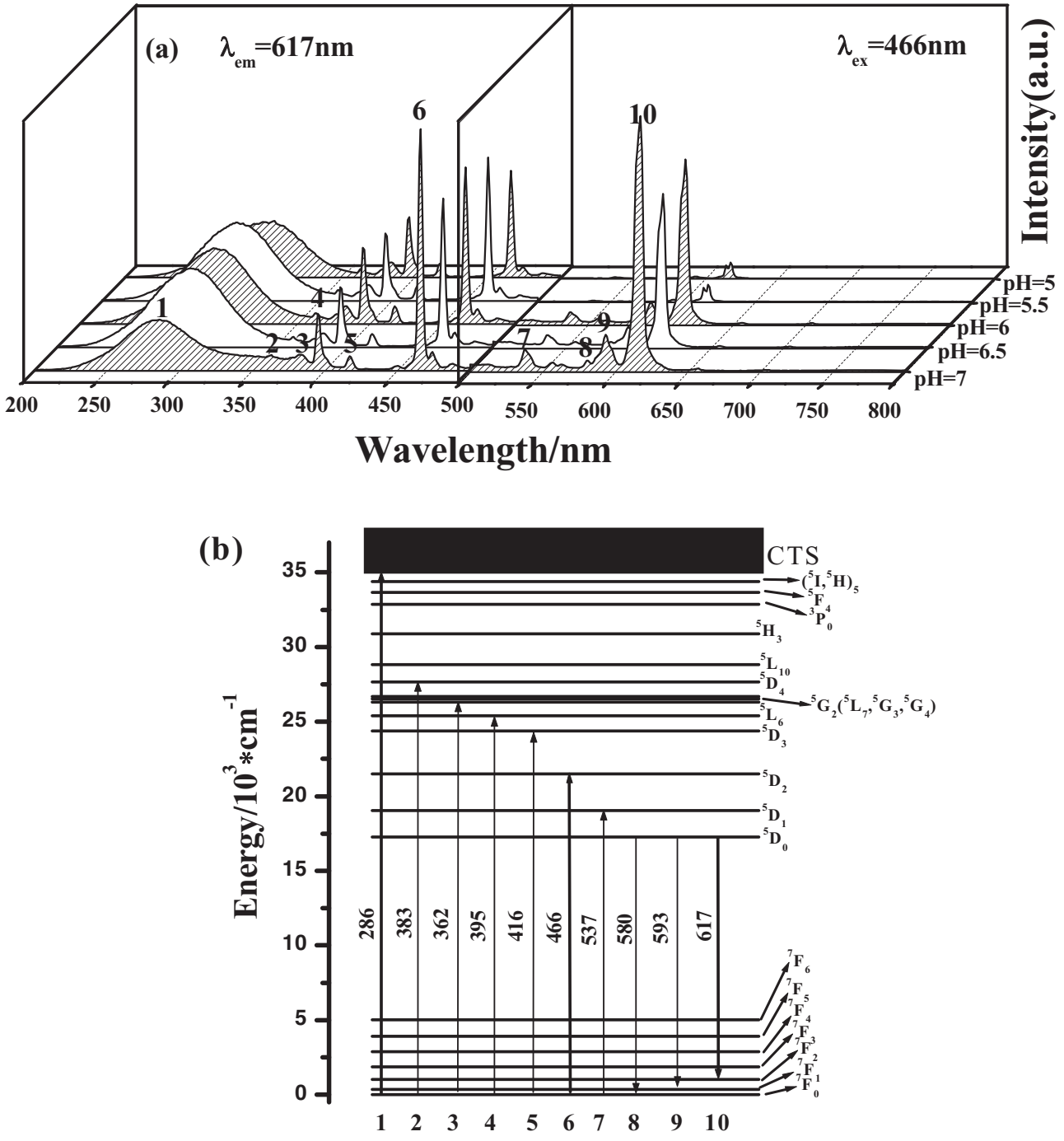

Figure 4. (a) the excitation(left) and emission(right) spectra of $NaY(MoO_4)_2$:Eu^{3+} with different pH values; (b) the transitions depicted from 1 to 10 of Eu^{3+}.

an emission wavelength of 617 nm for $^5D_0 \rightarrow {}^7F_2$ transition. We can see that the excitation spectrum shows a broad band in the range of 200-350 nm with the maximum centered around 286 nm, which can be ascribed to the host absorption of MoO_4^{2-} involving the charge transfer state (CTS) from O^{2-} to Mo^{6+}. This is also confirmed by the distribution of PDOS(Section 3.2). In addition, there are some strong sharp lines in the longer wavelength range of 350-500 nm and the sharp lines are associated with the typical intra-4f transitions of Eu^{3+} ion (Figure 4b).[28]

Generally, the emission spectra of Eu^{3+} are sensitive to the surrounding environment. A variation in the environment of the optically active Eu^{3+} ion can produce a modification in the number of observed $^5D_0$–^7F_J transitions, their relative intensity and the magnitude of the crystal field splitting for each ^7F_J state. When Eu^{3+} ions are embedded in sites with inversion symmetry, the $^5D_0$–$^7F_1$ magnetic dipole transition will dominate; on the contrary, when a Eu^{3+} ion site is non-centrosymmetric, the $^5D_0$–$^7F_2$ electric dipole transitions will be the strongest in the emission. In this case, $NaY(MoO_4)_2$ has a tetragonal scheelite structure with space group $I4_1/a$, in which Y^{3+} is coordinated with eight oxygen atoms and has a S_4 point symmetry with no inversion center. Upon 466 nm excitation, characteristic emission peaks of Eu^{3+} within the wavelength range from 580 nm to 655 nm

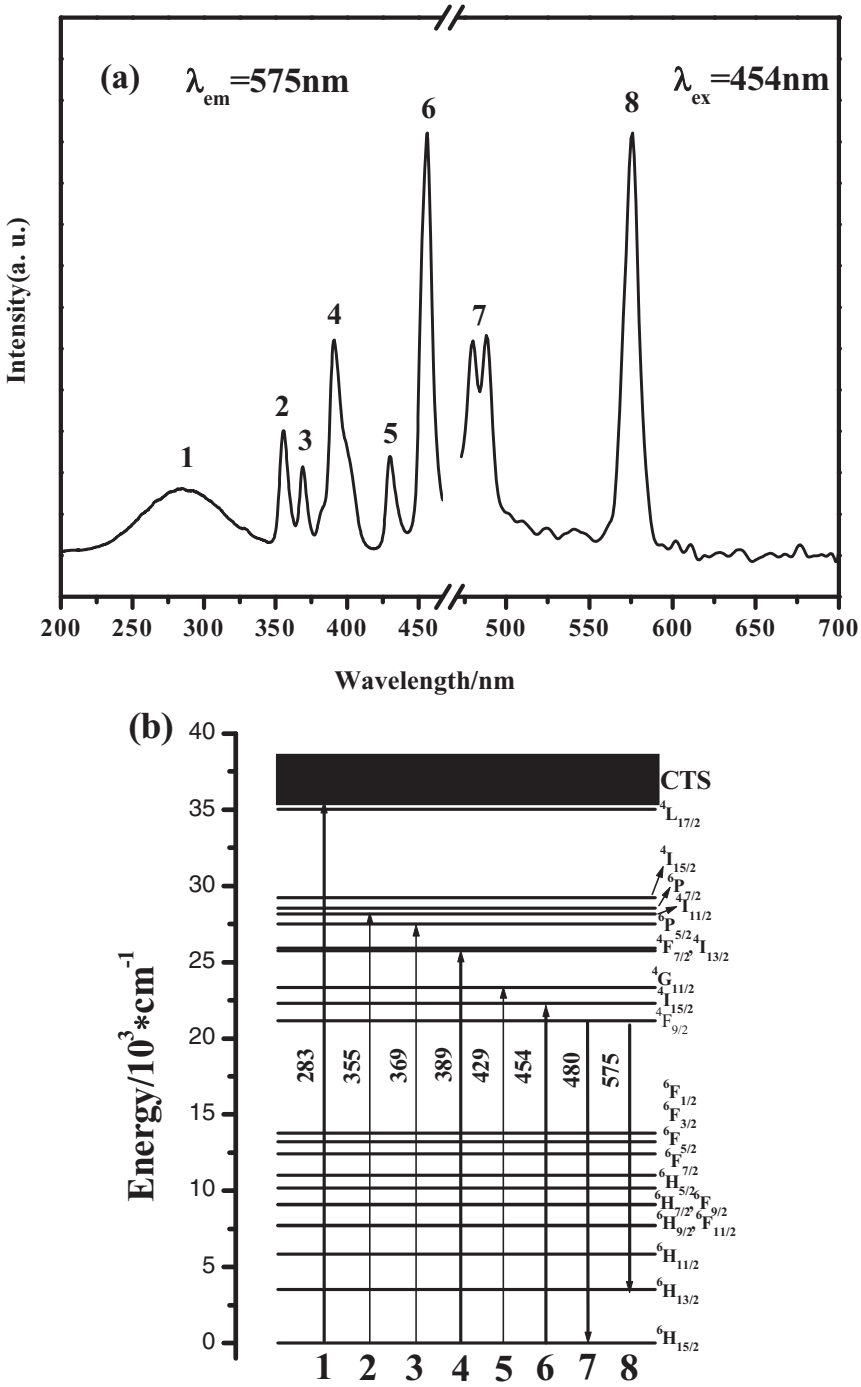

Figure 5. (a) the excitation(left) and emission(right) spectra of Dy^{3+}-doped $NaY(MoO_4)_2$; (b) the transitions depicted from 1 to 8 of Dy^{3+}.

are assigned to transitions from the excited $^5D_0$ state to ^7F_J (J = 0–3) levels (see Figure 4b). The emission spectrum is dominated by the red $^5D_0$–$^7F_2$ transition of Eu^{3+} at 617 nm, which corresponds to the electric dipole transition and indicates that the Eu^{3+} ions occupy a site without inversion symmetry in the crystal lattice. The emission color was also analyzed and confirmed with the help of CIE chromaticity coordinates. The chromaticity then corresponds to a red region in the CIE diagram (Figure 7a). In summary, the $NaY(MoO_4)_2$:Eu^{3+} phosphor in our experiment showed an intensive red emission under 466 nm excitation, indicating that it may be applied as an excellent red component for blue chip white LEDs.

Photoluminescent properties of $NaY(MoO_4)_2$:Dy^{3+}.— It is well known that the color of the trivalent dysprosium ($4f^9$ configuration) luminescence is close to white. Figure 5a shows the excitation and emission spectra of $NaY(MoO_4)_2$:Dy^{3+}. A similar excitation spectrum in the wavelength range from 200–500 nm as Eu^{3+} is obtained, in which the principal features are a strong excitation band extending from 200 to 320 nm with broad band maximum at 283 nm and some sharp peaks induced by the f–f transitions of Dy^{3+}.[29] Among all the excitation bands, the broad band (283 nm) corresponds to host absorption, while the peak located at 454 nm ($^6H_{15/2}$–$^4I_{15/2}$) has the maximum intensity. The 454 nm radiation excites the Dy^{3+} ions to the $^4I_{11/2}$ level and then quickly relaxes nonradiatively to populate the $^4F_{9/2}$ level.[30,31] The yellowish white light is composed of blue (480 nm) and yellow (575 nm) regions (Figure 5b). They correspond to the emission from the $^4F_{9/2}$ excited state to the $^6H_{15/2}$ and $^6H_{13/2}$ ground states, respectively. The $^4F_{9/2}$–$^6H_{13/2}$ is a hypersensitive

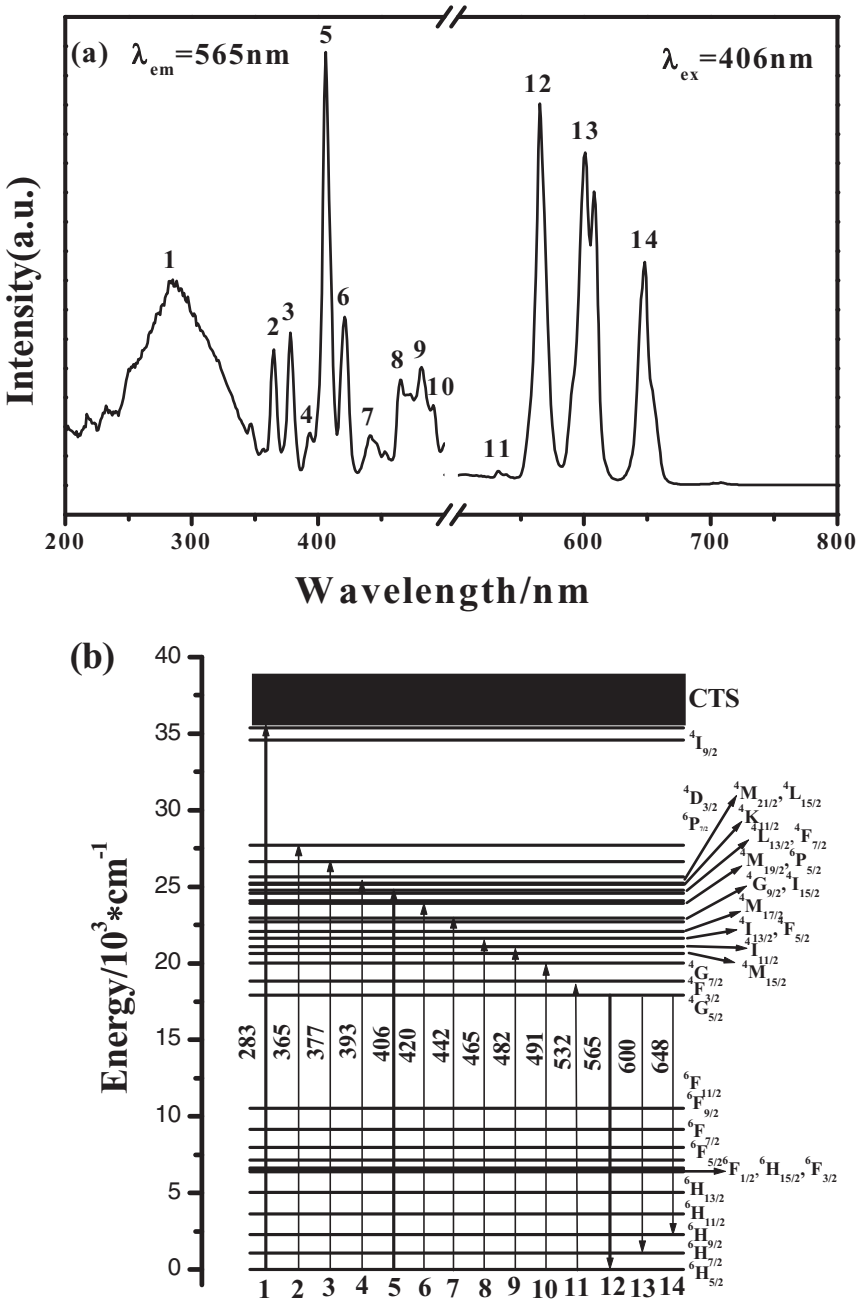

Figure 6. (a) the excitation(left) and emission(right) spectra of Sm^{3+}-doped $NaY(MoO_4)_2$; (b) the transitions depicted from 1 to 14 of Sm^{3+}.

transition ($\Delta J = 2$), which is strongly influenced by the surrounding environment around the Dy^{3+} ion. The $^4F_{9/2}$–$^6H_{13/2}$ forced electric dipole transition is predominant only when Dy^{3+} ions are located at low-symmetry sites with no inversion centers in $NaY(MoO_4)_2$, which is in accordance with the S_4 point symmetry. The CIE chromaticity coordinates for Dy^{3+}-doped $NaY(MoO_4)_2$ phosphors is located at (x = 0.336, y = 0.328), as indicated in the CIE diagram in Figure 7b. It is obvious that the coordinate is very close to the standard white illuminate.

Photoluminescent properties of $NaY(MoO_4)_2$:Sm^{3+}.— Trivalent samarium with $4f^5$ configuration has complicated energy levels and various possible transitions between 4f levels. The transitions between these 4f levels are highly selective and of sharp line spectra. The excitation and emission spectra of $NaY(MoO_4)_2$:Sm^{3+} are given in Figure 6a. We can see from Figure 6a that the excitation spectrum of sample is composed of a series of narrow peaks including 365, 377, 406, 421, 441, 465, 482 and 490 nm, which are attributed to the f–f transition of Sm^{3+} ions (Figure 6b). In addition, there is a wide excited band at the region of 200–350 nm with broad band maximum at 283 nm. Similarly, it is well known that this band is attributed to the host absorption. The emission spectrum of $NaY(MoO_4)_2$:Sm^{3+} consists of three groups of narrow band emissions including 550–575, 580–625 and 630–670 nm. All these emissions belong to the characteristic emission of Sm^{3+}.[22] The reason of generating the three emissions is the radiation transition from excited state of Sm^{3+} ion to three lower energy states, that is to say, from $^4G_{5/2}$ to $^6H_{5/2}$, $^6H_{7/2}$ and $^6H_{9/2}$ (Figure 6b). The luminous colors of the phosphors are reddish orange as result of complex spectra. In general, luminous color is represented by color coordinates and color ratios. At the present work, the values of chromaticity coordinate of the phosphor $NaY(MoO_4)_2$:Sm^{3+} has been calculated using the CIE system. It has been found that the sample has chromaticity coordinates of x = 0.518 and y = 0.314, which shows reddish orange light emission(Figure 7c).

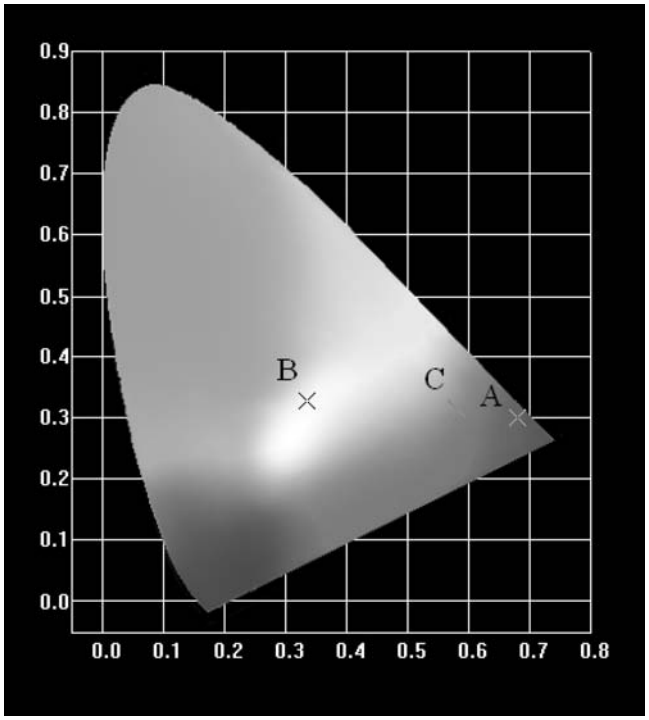

Figure 7. Chromaticity coordinates of $NaY(MoO_4)_2$:Eu^{3+}, $NaY(MoO_4)_2$:Dy^{3+}, $NaY(MoO_4)_2$:Sm^{3+} phosphors signed (A), (B) and (C), respectively.

Conclusion

In summary, novel phosphors, Eu^{3+}-, Dy^{3+}-, Sm^{3+}-doped $NaY(MoO_4)_2$ were synthesized by hydrothermal reaction with further calcinations. The crystal structure, morphology, and luminescence properties were characterized by XRD, FE-SEM, PL and diffused reflectance spectrum, respectively. It is conceived that their optical absorption of $NaY(MoO_4)_2$ at low energy region can be mainly ascribed to the charge transitions from O-2p to Mo-4d states. Our calculated value of the direct band gap for $NaY(MoO_4)_2$ is 3.46 eV by using DFT calculations, which is higher than the experimental value of 3.28 eV from the diffused reflectance spectra. Under blue excitation, the Eu^{3+}-, Dy^{3+}-, Sm^{3+}-doped $NaY(MoO_4)_2$ show strong red, white light and reddish orange, respectively. These phosphors can be used as a potential candidate for white-light-emitting diode and other display devices.

Acknowledgments

This work was supported by the National Science Foundation of China (no. 11004081), partially supported by a grant-in-aid for the Fundamental Research Funds for the Central Universities (no. 450060326085) and by the Science and Technology Innovation Projects of Jilin Province for overseas students and by the Korea Research Foundation Grant funded by the Korean Government (2010-0022540) and by the National Core Research Center Program from MEST and NRF(2010-0001-226) and by the Open Project of State Key Laboratory of Rare Earth Resources Utilization, Changchun Institute of Applied Chemistry, Chinese Academy of Sciences (RERU2011005).

References

1. V. Sivakumar and U. V. Varadaraju, *J. Electrochem. Soc*., **153**, H54 (2006).
2. G. Blasse, *J. Chem. Phys*., **45**, 2356 (1966).
3. Y. R. Do and Y. D. Huh, *J. Electrochem. Soc*., **147**, 4385 (2000).
4. C. Duan, J. Yuan, X. Yang, J. Zhao, Y. Fu, G. Zhang, Z. Qi, and Z. Shi, *J. Phys. D: Appl. Phys*., **38**, 3576 (2005).
5. A. Komeno, K. Uematsu, K. Toda, and M. Sato, *J. Alloys Compd*., **408–412**, 871 (2006).
6. A. H. Kitai, *Thin Solid Films*., **445**, 367 (2003).
7. V. Sivakumar and U. V. Vardaraju, *J. Electrochem. Soc*., **152**, H168 (2005).
8. X. X. Zhao, X. J. Wang, B. J. Chen, Q. Y. Meng, B. Yan, and W. H. Di, *Opt. Mater.*, **29**, 1680 (2007).
9. F. Lei and B. J. Yan, *Solid State Chem*., **181**, 855 (2008).
10. S. Neeraj, N. Kijima, and A. K. Cheethanl, *Chem. Phys. Lett*., **387**, 2 (2004).
11. C. F. Guo, T. Chen, L. Luan, W. Zhang, and D. X. Huang, *J. Phys. Chem. Solids*., **69**, 1905 (2008).
12. Y. K. Voron'ko, K. A. Subbotin, V. E. Shukshin, D. A. Lis, S. N. Ushakov, A. V. Popov, and E. V. Zharikov, *Opt. Mater.*, **29**, 246 (2006).
13. X. Z. Li, Z. B. Lin, L. Z. Zhang, and G. F. Wang, *J. Cryst. Growth*, **290**, 670 (2006).
14. X. A. Lu, Z. Y. You, J. F. Li, Z. J. Zhu, G. H. Jia, B. C. Wu, and C. Y. Tu, *J. Alloys Compd*., **426**, 352 (2006).
15. L. Macalik, J. Hanuza, J. Sokolnicki, and J. Legendziewicz, *Spectrochim. Acta A*, **55**, 251 (1999).
16. C. F. Guo, S. T. Wang, T. Chen, L. Luan, and Y. Xu, *Appl. Phys. A*., **94**, 365 (2009).
17. C. Cascales, A. M. Blas, M. Rico, V. Volkov, and C. Zaldo, *Opt. Mater.*, **27**, 1672 (2005).
18. X. Z. Li and G. F. Wang, *Chinese J. Struct. Chem*., **25**, 392 (2006).
19. Z. L. Wang, H. B. Liang, M. L. Gong, and Q. Su, *Opt. Mater.*, **29**, 896 (2007).
20. M. D. Segall, J. D. L. Philip, M. J. Probert, C. J. Pickard, P. J. Hasnip, S. J. Clark, and M. C. Payne, *J. Phys.: Condens. Matter*, **14**, 2717 (2002).
21. D. Vanderbilt, *Phys. Rev. B*., **41**, 7892 (1990).
22. H. J. Monkhorst and J. D. Pack, *Phys. Rev. B*., **13**, 5188 (1976).
23. D. M. Ceperley and B. J. Alder, *Phys. Rev. Lett*., **45**, 566 (1980).
24. J. P. Perdew and A. Zunger, *Phys. Rev. B*., **23**, 5048 (1981).
25. D. Vanderbilt, *Phys. Rev. B*., **41**, 7892 (1990).
26. P. Kubelka, *J. Opt. Soc. Am*., **38**, 448 (1948).
27. D. Zhao, W.-D. Cheng, H. Zhang, S.-P. Huang, M. Fang, W.-L. Zhang, and S.-L. Yang, *J. Mol. Struct*., **919**, 178 (2009).
28. Y. C. Li, Y. H. Chang, Y. F. Lin, Y. S. Chang, and Y. J. Lin, *J. Alloys Compd*., **439**, 367 (2007).
29. B. V. Ratnam, M. Jayasimhadriz, K. Jang, and H. S. Lee, *J. Am. Ceram. Soc*., **93**, 3857 (2010).
30. Y. N. Xue, F. Xiao, Q. Y. Zhang, and Z. H. Jiang, *J. Rare. Earth*., **27**, 753 (2009).
31. Y. L. Liu, B. F. Lei, and C. S. Shi, *Chem. Mater.*, **17**, 2108 (2005).